

MAGNETIC AND ELECTRIC FIELD WAVES IN SLOW SHOCKS OF THE DISTANT GEOMAGNETIC TAIL: ISEE 3 OBSERVATIONS

F. V. Coroniti, S. I. Moses, and E. W. Greenstadt
TRW Space and Electronics Group, Redondo Beach CA

B. T. Tsurutani and E. J. Smith
California Institute of Technology, Jet Propulsion Laboratory, Pasadena CA

Abstract. During ISEE 3's first pass through the distant geomagnetic tail, the slow shocks encountered on February 2 and 11, 1983 provide particularly clear examples of the magnetic field and plasma wave properties of the shock transition. The magnetic ramp contains transverse polarized magnetic field oscillations with frequencies just below the ion cyclotron frequency and amplitudes of 2 to 4 nT. These waves are plausibly generated by the electromagnetic ion/ion cyclotron instability predicted by *Winske and Omidji [1990]*. The electric field plasma waves within the shock ramp exhibit two spectral peaks. A mid-frequency emission occurs near the ion plasma frequency and electron cyclotron frequency, but well below the maximum Doppler shift frequency for electrostatic waves. The mid-frequency waves extend into the upstream region where the spectral peak occurs at a slightly higher frequency. A new high frequency emission with frequencies between the maximum Doppler shift frequency and the electron plasma frequency occurs throughout the downstream region. This emission disappears at the start of the magnetic ramp, and is replaced upstream by electron plasma oscillations. The high frequency emissions are clearly polarized parallel to the magnetic field. The polarization of the mid-frequency waves is less certain; both parallel and a fairly broad angular distribution about the parallel electric fields are consistent with the measurements.

1. Introduction

The ISEE 3 passes through the distant geomagnetic tail provided the first identification of slow shocks which hydromagnetic models of reconnection predict should stand in the upstream flow and bound the plasma sheet [*Feldman et al.*, 1984, 1985]. As in fast mode shocks, plasma wave turbulence occurs in both the upstream and downstream regions of the distant tail slow shocks [*Scarf et al.*, 1984]. Within the slow shock's magnetic ramp and extending into the upstream flow, the electric field wave emissions exhibit a relatively narrow band peak near, but usually above, the ion plasma frequency which resembles the waves detected in fast shocks [*Gurnett,*

198 S]. Upstream, electron plasma oscillations often occur in association with the heat flux carried by shock-heated electrons escaping along the magnetic field lines. A search for lower hybrid emissions, which are potential sources of anomalous resistance, failed to detect the magnetic component of these waves [Coroniti et al., 1988].

The previous studies of waves in the slow shocks emphasized the average spectral characteristics of the emissions; neither the high time resolution structure of the slow shock electric or magnetic field waves, nor the electric field polarization were investigated. In this paper we carry out these heretofore neglected investigations. Section 2 discusses the average E-field spectral changes which occurred during two ISEE-3 slow shock encounters in February, 1983. In Section 3 we present high time resolution magnetic field and plasma wave measurements. Large amplitude nearly transverse magnetic field perturbations occur within the magnetic field shock ramp. The mid-frequency, narrowband plasma waves are highly impulsive, and occur both in the upstream and down stream regions. We also identify a new high frequency wave mode which occurs in the magnetic ramp, but disappears in the upstream region. Section 4 discusses the electric field polarization characteristics, and Section 5 offers some comments on these measurements.

2. Slow Shock Spectra

The two slow shocks occurred on February 2 and 11, 1983 when ISEE-3 was located in the distant tail about 220 R_J downstream. The upstream and downstream plasma parameters for these shocks are given in Feldman et al. [1985] and Schwartz et al. [1987]; both shocks had Alfvén Mach numbers and propagation angles to the upstream field that correspond to nearly switch-off slow shock conditions. For the February 2 shock the upstream (down stream) plasma density, electron temperature, flow speed, and magnetic field strength are $n_1 = 0.3 \text{ cm}^{-3}$ ($n_2 = 0.5 \text{ cm}^{-3}$), $T_{e1} = 3.3 \times 10^5 \text{ K}$ ($T_{e2} = 8 \times 10^5 \text{ K}$), $v_{x1} = 210 \text{ km/s}$ ($v_{x2} = 530 \text{ km/s}$), and $B_1 = 10.8 \text{ nT}$ ($B_2 = 3 \text{ nT}$). For the February 11 shock the corresponding parameters are $n_1 = 0.27 \text{ cm}^{-3}$ ($n_2 = 0.750 \text{ cm}^{-3}$), $T_{e1} = 7 \times 10^5 \text{ K}$ ($T_{e2} = 1.8 \times 10^6 \text{ K}$), $v_{x1} = 90 \text{ km/s}$ ($v_{x2} = 750 \text{ km/s}$), and $B_1 = 19 \text{ nT}$ ($B_2 = 4 \text{ nT}$). The downstream ion temperatures inferred from pressure balance between the upstream field strength and downstream plasma pressure is $T_{i2} = 0.6 \text{ keV}$ ($T_{i2} = 1.25 \text{ keV}$) for the February 2 (11) shocks.

In the discussion below we refer to the following characteristic wave frequencies; $f_c = 28 B(\text{nT}) \text{ Hz}$ is the electron cyclotron frequency; $f_{pe} = 9 n^{1/2} \text{ kHz}$ is the electron plasma frequency; and $f_{pi} = 210 n^{1/2} \text{ Hz}$ is the ion plasma frequency for hydrogen. The lower hybrid frequency is typically below the lowest electric field frequency channel (17.8 Hz) of the TRW/U. low plasma wave

detector. The maximum Doppler shift frequency for a wave with wave number k is $f_D = k\lambda_D (v/v_e)f_{pe}$ where $v = v_x$ is the flow speed, $v_e = (T_e/m_e)^{1/2}$ and $\lambda_D = v_e/(2\pi f_{pe})$ is the Debye length.

Slow Shock on February 2, 1983

Figure 1 displays nine selected peak (top curves) and 30-second average (bottom curves) electric field amplitude spectra (volts/m-Hz^{1/2}) for the February 2, 1983 slow shock. For reference the magnetic field strength (B) and the x-component (B_x) are shown in the center; detailed field profiles can be found in *Coroniti et al.* [1988]. The three bottom spectra were obtained between 1924:37 UT to 1935:00 UT when the spacecraft was in the region upstream of the shock. The narrow peaked emissions at 5.6 kHz are electron plasma oscillations which are presumably excited by shock-heated electrons that escape upstream. The plasma oscillations terminate at 1947 UT when the escaping electron heat flux abruptly decreased [Feldman et al., 1985] in the mid-frequency range (50 -500 Hz), the spectra exhibit a strong peak near 178-316 Hz; in contrast to the broad power law spectra of broad band electrostatic noise (BEN) [Gurnett et al., 1976; Grabbe and Eastman, 1984] this mid-frequency emission has been termed narrowband electrostatic noise (NEN) [Coroniti and Ashour-Abdalla, 1989]. The NEN peak is above the upstream ion plasma frequency ($f_{pi} = 115$ Hz), and near, but below, the upstream electron cyclotron frequency ($f_c = 300$ Hz). The upstream Doppler frequency is $f_D = 460 k\lambda_D$ Hz. The upstream NEN also continues to 1947 UT, and diminishes with the decrease in the electron heat flux.

The 1922:27 UT spectrum was obtained midway through the magnetic shock ramp. The electron plasma oscillations have disappeared, and a slight amplitude enhancement has developed between 1.78 and 5.6 kHz. In the 1920:50 UT spectrum taken at the bottom of the ramp, this slight enhancement has become a definite second peak in both the average and peak spectra, and this high-frequency emission is clearly separated from the mid-frequency NEN peak by a break or dip in the spectral slope. The maximum of the NEN now occurs between 100 and 178 Hz, but is clearly below the peak frequency of the upstream BEN. At 1920:50 the characteristic wave frequencies are $f_{pi} = 115$ Hz, $f_c = 140$ Hz and $f_D = 730 k\lambda_D$ Hz.

The 1919:12 UT spectrum was obtained just before the start of the shock ramp, on the plateau in magnetic field strength ($B = 3$ nT); the field strength is about equally divided between the B_x and B_y components. Both the NEN and high frequency peaks have decreased, but are still clearly discernible. At 1917:02 UT, the NEN spectral peak has disappeared, but the high frequency emission is still present. Although the field strength remains near 3 nT, B_x is nearly zero, and the

total field is carried by the B_y component. The vanishing of B_x corresponds to the downstream state of the switch-off shock. Finally, the 1914:20 UT spectrum was obtained on the other side of the B_x reversal ($B_x < 0$ to $B_x > 0$), but still on the magnetic plateau. The high frequency and NEN spectral peaks are at frequencies of 3.16 kHz and 178 Hz, respectively, and the break in spectral slope between the two emissions occurs at 1 kHz, which equals the maximum Doppler shift frequency for waves with $k\lambda_D = 1$.

Slow Shock on February 11, 1983

Figure 2 displays selected frequency spectra and the magnetic field (B and B_x) for the slow shock encountered at 2025 to 2030 UT on February 11, 1983. The 2031:05 UT spectra exhibits the upstream plasma oscillation peak at 5.6 kHz and the NEN peak near 178-316 Hz. The upstream ion plasma frequency was $f_{pi} = 110$ Hz, whereas the electron cyclotron frequency was $f_c = 540$ Hz, which is well above the NEN peak. In the 2028:5 UT spectrum measured at the start of the magnetic ramp, the electron plasma oscillations have disappeared, and a weak peak has developed between 1.75 and 3.16 kHz. At the base of the magnetic ramp (2027:50 UT spectrum) this high frequency emission clearly extends from 1 kHz to at least 10 kHz. The maximum Doppler shift frequency is $1.1 k\lambda_D$ kHz, and the downstream electron plasma frequency is 7.8 kHz; thus the high frequency emission cannot simply be the result of Doppler up-shifting of low frequency waves. The NEN amplitudes maximize between 100 Hz and 178 Hz which is lower than the NEN upstream peak frequency; the NEN frequencies are still below the local electron cyclotron frequency (approximately 280 Hz) but are now comparable to the downstream ion plasma frequency.

The mid- and high frequency components persist in the downstream flow and are still discernable (2022:57 UT spectrum) after the magnetic field strength decreases to 4.5 nT (2025 UT). The NEN spectral peak remains near 100-178 Hz, and is now close to the local electron cyclotron frequency. At 2022:25 UT, both B_x and B_y are nearly zero, and the field magnitude is carried by the $B_z = -4$ nT component. In the 2022:25 UT spectrum, the NEN peak has disappeared and the high frequency emission is barely (if at all) perceptible.

Discussion

Downstream of the leading edge decrease in the magnetic field, the wave spectra in both slow shocks exhibit distinct mid- and high frequency peaks. A spectral break separates the two emissions and the frequency of the break is close to the maximum Doppler shift frequency for

modes with $k\lambda_D = 1$. The spectra of these two emissions strongly resemble the wave spectra detected downstream of the low Mach number fast shocks on the flanks of the magnetosphere [Coroniti *et al.*, 1993]. In both the fast and slow shock spectra, the high frequency signals start near f_D and extend up to the local electron plasma frequency; we show below that the high frequency modes in the slow shocks are also polarized along the magnetic field.

in the weak flank bow shocks, the mid-frequency waves occurred at frequencies well above the downstream electron cyclotron frequency, near or just above the ion plasma frequency, and well below the maximum Doppler shift frequency; however, the downstream plasma and magnetic field values did not vary greatly for the fast shocks studied by Coroniti *et al.* [1993]. For the two February 1983 slow shocks, the upstream NEN spectral peak was close to the local electron cyclotron frequency for one shock, but well below f_c for the other; in both cases the peak was above the upstream ion plasma frequency. Downstream the NEN peak occurs at a lower frequency, and is close to both f_c and f_{pi} . Since f_{pi} increases across the slow shock, the NEN peak frequency does not scale (in any obvious way) with density. The peak frequency could scale with magnetic field strength; however, since the two slow shocks had quite different upstream field strengths but the same NEN spectral peak frequencies, the emission is apparently not controlled (at least significantly) by the magnetic field strength. Curiously, in both slow shocks, the mid-frequency emission disappears when B_x vanishes, even though the magnetic field strength remained constant during the B_x sign reversal interval.

Finally, the peak NEN frequency is clearly anti-correlated with the maximum Doppler shift frequency, which increases strongly from upstream to downstream in the slow shock. The anti-correlation suggests that the mid-frequency signals are not significantly Doppler shifted. There are (at least) two possible ways to avoid Doppler shifting. Firstly, if the wavelengths are so long that $f_D \ll f$, the measured mode frequencies will be unaffected by the flow. For the downstream NEN, $f_D \ll f$ requires $k\lambda_D < 1/10 - 1/20$. The second possibility is that the waves do not couple to the bulk ion flow, but, for example, only to the electron species; the electron velocity space hole modes proposed by Coroniti and Ashour-Abdalla [1989] and very cold fast ion beam modes [Grabbe and Eastman, 1984] have this property, but ion acoustic waves do not. The mid-frequency waves detected in the magnetosheath, which spectrally resemble NEN, have measured or inferred wavelengths of $k\lambda_D = 0.1 - 1.0$ [Rodríguez, 1979; Anderson *et al.*, 1982; Gallagher, 1985], and are usually assumed or inferred to be ion acoustic waves [Gallagher, 1985]. Whether the magnetosheath emissions and NEN are physically related is, however, undetermined.

3. High Time Resolved Slow Shock Structure

February 2, 1983 Slow Shock

Figures 3a,b,c display the magnetic field at the highest time resolution of 1/6 second per vector and the plasma wave E-field amplitudes measured every 0.5 second for the ramp interval of the February 2, 1983 slow shock. From 1918 to 1919 UT (Figure 3a) B_x and B_z are near zero, and the 3 to 4 nT field strength is carried in the B_y component; just before 1918 B_x changed sign (to positive), so that the B_x near zero period after 1918 UT would represent the downstream end of the slow shock transition. The mid-frequency wave signals are very weak, and the high frequency intensities are low but clearly present. At 1918:40 UT oscillations began in B_z . The mid-frequency wave amplitudes abruptly increased at 1919 UT just when the magnetic field strength started to increase in the ramp. During the next minute, the bursts of mid-frequency emissions became more frequent so that after 1920 UT these signals are nearly continuous although temporally impulsive. The high frequency waves exhibit a clear modulation of the amplitude at twice the ISM spin frequency (the spin period is about 3 s) which indicates that the waves are highly polarized. The mid-frequency wave amplitudes also occasionally show ripple at twice the spin frequency (e.g. near 1921 UT).

After 1919 UT, the B_y and B_z components developed quite regular oscillations with peak-to-peak amplitudes of 1 to 2 nT. Although somewhat similar and less regular, oscillations also occur in B_x and the field strength. The field oscillations have periods between 8 to 12 seconds which, in the 5 to 8 nT field, are comparable to the ion gyroperiod. Thus these magnetic oscillations might be the ion cyclotron waves which Winske and Omid [1990] and Omid and Winske [1992] observed in hybrid simulations of slow shocks. In the simulations escaping downstream ions interact in the upstream region with the cold incoming ions via the electromagnetic ion/ion cyclotron instability. The excited waves can be convected into the downstream region and even disrupt the shock structure, making the shock unsteady.

Figure 3b presents the high resolution measurements from the middle to top of the slow shock's magnetic ramp. At low frequencies the 56 Hz E-field amplitudes gradually diminish toward the upstream direction. The mid-frequency emissions maintain the same signal strength and temporal character throughout the ramp; note that the electron cyclotron frequency passes from below (at 1922 UT) to above (at 1926 UT) the 316 Hz channel without significantly affecting these emissions. The high frequency wave amplitudes slowly decrease, and the 1.78 kHz and 3.16 kHz channels approach background after 1925 UT. The spin ripple in these channels abruptly stops at 1924:40 UT. The emissions in the 5.62 kHz channel change character between 1923 and 1925

UT, becoming temporally more impulsive. After 1924:40 UT, the wave spectra show that the 5.62 kHz signals are narrowband electron plasma oscillations. *Feldman et al.* [1985] show that the electron density and temperature jumps occur about 1923 to 1924 UT which corresponds to the cessation of the high-frequency emissions and the onset of electron plasma oscillations at 5.62 kHz. The magnetic oscillations in all components continued during the shock ramp until 1924 UT. The peak-to-peak fluctuation amplitude is about 4 nT in B_y and B_z , about 2 nT in B_x and 1.5 nT in B . (Note the different scales in Figure 3b and the change in scale from Figure 3a.) After 1924 UT the oscillation amplitude in B_x became quite small.

The measurements from the immediate upstream region are displayed in Figure 3c. Magnetic fluctuations continue with reduced, < 1 nT, amplitudes. At 1929:40 UT B_y develops a new and more regular oscillation with a period of about 10 seconds; the local ion cyclotron period is about 6 seconds. The B_x and B_z components exhibit very little variation at this time; thus, the magnetic wave is nearly linearly polarized, which is consistent with the *Winske and Omidi* [1990] prediction for the electromagnetic ion/ion cyclotron instability. A few minutes after 1930 UT, (see Figure 1 of *Coroniti et al.* [1988]) B_y and B_z do develop coherent and nearly equal amplitude oscillations which are probably the ion-driven right-hand magnetosonic waves discovered by *Tsurutani et al.* [1985].

In the electric field measurements, both the ion-frequency and electron plasma oscillations persist upstream. At low frequencies, impulsive emissions at 56 Hz and 1001 Hz commence at 1928 UT. Interestingly, just after the first cycle of the strong B_y oscillations, the plasma emitted a strong broadband (56 Hz to 5.6 kHz) burst of electrostatic noise. *Winske and Omidi* [1990] have speculated that electromagnetic ion/ion cyclotron unstable waves might nonlinearly trap ions and thus create free energy which could excite higher frequency electrostatic waves.

February 11, 1983 Slow Shock

Figures 4 a,b display the high resolution magnetic field and E-field measurements from 2022 to 2030 UT for the February 11, 1983 slow shock crossing. The B_x component passes through zero at 2022:35 and remains close to zero until 2022:42 UT. At 2022:35 UT B_z and the field strength sharply increase from 1 nT to 5 nT. At 2023 UT B_x increases as $|B|$ diminishes so that the field magnitude remains relatively constant at a plateau value of 4 nT from 2023 to 2024:30 UT. Although the magnetic field fluctuates during this interval, the oscillations do not have a clear wave-like character. Before 2023:09 UT, the E-field amplitudes are low and fairly constant in all frequency channels. At 2023:09 UT, when the $|B_x|$ ($|B_z|$) increase (decrease) is completed, the

mid-frequency amplitudes suddenly exhibit a sharp spike, and then gradually increase in amplitude and temporal variability.

Just after 2024 UT, B_X anti the magnetic field strength increase to a second plateau value of about 10 nT. The field magnitude and components now exhibit wave-like oscillations with periods of 10 to 15 seconds and peak-to-peak amplitudes of about 4 nT in the components and 1.5 nT in the magnitude. The local ion cyclotron frequency is 6 seconds, so that the wave properties are consistent with being ion cyclotron waves. During the second magnetic plateau interval, the E-field emissions increased in intensity and temporal variability. The high frequency signals are often modulated at twice the satellite spin frequency; near 2025:50 UT, the 56 to 178 Hz channels also exhibit spin modulation.

At 2028 UT the magnetic field starts the final ramp to the upstream value. The magnetic oscillations diminish in amplitude, and disappear just after 2030 UT (not shown). During the ramp the high frequency plasma waves decrease in amplitude, and the emission drops below 10 kHz after 2028:40 UT. At this time the electron plasma frequency is about 5.6 kHz; however the high frequency signals remain broadband and there is no evidence of electron plasma oscillations. The amplitudes of the mid-frequency waves also decrease toward the upstream region.

Discussion

The downstream regions of both slow shocks have very similar magnetic field and plasma wave activity. In the leading edge of the ramp the electron plasma oscillations that appear upstream abruptly cease, and are replaced by a broadband high frequency emission which is spin modulated. The mid-frequency waves are strong throughout the ramp but weaken significantly and/or disappear when B_X goes to zero downstream. Strong magnetic oscillations with frequencies below the ion cyclotron frequency occur throughout the ramp, but disappear upstream.

The slow shock simulations of *Winske and Omid* [1990] and *Omid and Winske* [1992] have many features which closely resemble the magnetic profiles and oscillations observed in the February 2 and 11, 1983 slow shocks. In the simulations the overall shock scale length, defined as the separation between the initial decrease in magnetic field strength to the downstream vanishing of the tangential field component, is roughly $50 c/\omega_{pi}$ based on the upstream density. For the tail slow shocks $50 c/\omega_{pi}$ corresponds to 3 RE. Both shocks took approximately eight minutes to go from upstream to downstream; if the shock thickness is $3R_E$, this traversal time would imply a shock speed of 40 km/s. A plasma sheet thickness of $3R_E$ and speed of 40 km/s

are reasonable in the distant tail [Richardson and Cowley, 1985; Richardson et al., 1989]. Furthermore, the slow shocks in the tail should have significantly larger propagation angles relative to the upstream field ($\theta = 80^\circ$ to 85°) than the slow shocks studied in the simulations ($\theta = 60^\circ$). Since the shock heated ions would be better confined by the higher field inclination angles, the scale length of the tail slow shocks could be considerably smaller than in the simulation shocks.

The magnetic oscillations observed in the tail slow shocks are similar to the Alfvén waves excited by the electromagnetic ion/ion instability in the simulation shocks. In both cases, the magnetic waves begin at the leading edge of the magnetic ramp and continue throughout the shock transition. The wave amplitudes in the tail shocks relative to the upstream field strength are of order $\delta B_y/B = 0.1$ to 0.2 whereas in the simulations the amplitudes are somewhat higher $\delta B_y/B = 0.2$ to 0.5 . In the nonlinear evolution of the electromagnetic ion/ion instability [Winske and Omidi, 1992], the ion fluctuation velocity in the wave field (roughly δv_y proportional to δB_y) is eventually converted into random thermal motion by nonlinear wave breaking and phase space mixing. Hence the lower wave amplitudes observed in the tail slow shocks may imply that the wave instability may not be as effective in heating the upstream ions to the required downstream Rankine-Hugoniot temperature as in the simulation shocks.

4. Wave Electric Field Polarization

For both the February 2 and 11 slow shocks the magnetic field direction and magnitude changed sufficiently slowly that meaningful electric field polarization measurements can be made. The ISFE3 antenna is in the spin plane (the x-y plane), and six B-field measurements are obtained in one spin period. For most of the slow shock encounters, the magnetic field was predominantly in the x-y plane, so that the rotating antenna sampled both the parallel and perpendicular components of the wave electric fields. In the polarization plots displayed in Figures 5-8, the projection of the magnetic field on the spin plane is shown by the solid line labeled B. The radial distance from the origin is proportional to the logarithm of the electric field spectral amplitude (actually the voltage in the automatic gain control, AGC, amplifier) and the radial scale covers five decades. Each polarization plot contains two minutes or 240 measurements of the electric field. The direction of the sun (positive x) is toward the left and dusk (positive y) is toward the bottom.

High Frequency Emission

Figure 5 displays four successive polarization measurements for the 3.16 kHz 11-field channel for the interval 1914 UT to 1922 UT during the February 2, 1983 slow shock traversal; during this period the high frequency emission is centered at 3.16 kHz. Between 1914 UT to 1918 UT, the spacecraft was located on the opposite side of the neutral sheet or B_x reversal from the slow shock. The peak spectral amplitudes clearly occur when the antenna is oriented more nearly parallel to the magnetic field; the ratio of the maximum parallel to perpendicular amplitudes is about 10. Between 1916 UT and 1918 UT, the satellite was very close to the center of the plasma sheet, and the magnetic field and E-field polarization were predominantly in the y direction. From 1918 UT to 1922 UT the magnetic field rotated from being along y to its dominant direction in the shock ramp along x, and the peak E-field amplitudes followed the magnetic field direction change. The bottom two panels in Figure 6 display the 3.16 kHz polarization measurements for the February 11, 1983 slow shock; once again, the peak amplitudes occur preferentially along the field and follow the changing field direction.

The high frequency emission is clearly polarized parallel to the magnetic field. Recall that this field-aligned polarization was apparent in the previous high time resolution plots as a modulation of the channel amplitudes at twice the spin frequency. In the ISF3 measurements of the low Mach number fast bow shock in the distant flank region, the high frequency emissions detected in the downstream region, which are spectrally similar to those in the slow shock, were also polarized parallel to the magnetic field. Thus the fast and slow shock high frequency modes may have a common origin.

Mid-frequency Emission

Figure 6 presents four polarization measurements of the mid-frequency emissions obtained during the February 2, 1983 slow shock. The top (bottom) two panels show the 178 (316) Hz amplitudes which are the peak amplitude channels during the measurement interval. At 1914 UT the highest amplitudes clearly occurred when the antenna was oriented parallel to the magnetic field. From 1920 UT through 1930 UT, which corresponds to the shock ramp and near upstream region, the magnetic field is oriented nearly along the x-direction. The E-field amplitudes do not exhibit a visually apparent polarization direction, although the largest amplitudes do occur when the antenna is more nearly parallel to the magnetic field. In Figure 7 the top panels display the 178 Hz polarization measurements for the February 11, 1983 slow shock. The downstream (2022 UT) mid-frequency emissions are polarized along the field whereas the signals from the plateau in the shock ramp (2026 UT) do not have an apparent polarization; the polarization measurements in the steep shock ramp (not shown) are almost identical to those at 2026 UT.

The clear detection of a wave polarization using channel amplitudes, however, can be obscured if the signal strength has very large and rapidly fluctuating changes. The mid-frequency emissions are highly impulsive with peak-to-valley amplitude changes of 10^2 to 10^3 in a few measurement cycles. Suppose that the mid-frequency waves are actually polarized with the electric field exactly along the magnetic field. If a very high peak amplitude occurs when the antenna is nearly perpendicular to the magnetic field, its projection onto the antenna direction can still result in an electric field amplitude measurement which significantly exceeds the average value. If the next impulsive emission has a lower amplitude, but the antenna is now oriented along the magnetic field, the perpendicular and parallel emissions can appear to have the same amplitude, and the signal will appear to be unpolarized. Since the above polarization diagrams display the logarithm of the amplitude, the polarization of the impulsive signals is even more difficult to visually discern.

Figure 8 displays the polarization measurements of the mid-frequency emissions (1.78 and 3.16 Hz), the high frequency emission (3.16 kHz), and electron plasma oscillations (5.6 kHz) at the start of the shock ramp (1920 UT) and the near upstream region (1922 UT) for the February 2, 1983 slow shock. Superposed on the amplitude measurements, we have drawn two curves. The inner circle corresponds to the average electric field amplitude for the two minute interval over which the 240 sample measurements were obtained. The outer curve was constructed by first taking the largest E-field amplitude $E_p(\phi_p)$ (or voltage $V_p(\phi_p)$) measured during the two minute interval at angle ϕ_p between the antenna and magnetic field. We then project it back to the magnetic field direction as $E_p(\phi_p = 0) = E_p(\phi_p) / \cos(\phi_p)$ ($V_p(\phi_p = 0) = V_p(\phi_p) + (1/b) \ln(1/\cos(\phi_p))$) where b is a calibration constant. The outer curve is then given by the function $V(\phi) = V_p(\phi = 0) - (1/b) \ln(1/\cos(\phi))$. If the wave emission is polarized parallel to the magnetic field, there should be no E-field (voltage) values outside of the curve $V(\phi)$ at any ϕ .

First consider the 3.16 kHz polarization diagram at 1920 UT in Figure 8 (which is also displayed in Figure 5). The region between the peak $V(\phi)$ and average curves is fairly uniformly populated even though, from Figure 5, the high frequency emission is clearly polarized along the magnetic field. Although there are many measurements with ϕ near 90, only one value lies just slightly outside the $V(\phi)$ curve. If the wave electric fields were not strongly aligned with the magnetic field, we should observe some signals near $\phi = 90$ with amplitudes exceeding $V(\phi)$. Next consider the 5.6 kHz electron plasma oscillations at 1928 UT. It is commonly thought that plasma oscillations are parallel polarized since the most likely excitation sources are field-aligned electron beams. The 5.62 kHz polarization diagram, however, does not give a strong visual impression that these waves are parallel polarized. The plasma oscillations are highly impulsive signals with

large peak-to-valley ratios, thus making a polarization determination difficult. The only indication that the plasma oscillations are parallel polarized is the absence of large amplitude signals outside the $V(\phi)$ curve near $\phi = 90^\circ$.

Finally consider the mid-frequency polarization diagrams. Visually these diagrams are not significantly different than the 5.62 kHz plasma oscillation case; there is a definite absence of high amplitude signals near 90° . Thus, although the polarization diagrams do not prove that the mid-frequency waves are polarized along the magnetic field, the polarization measurements are consistent with parallel polarization given the highly impulsive nature of the emissions.

5. Discussion

The slow shocks in the distant geomagnetic tail exhibit a coherent internal structure in both their magnetic field oscillations and plasma wave properties. Within the shock ramp, the magnetic waves have frequencies which are comparable (0.5 to 1.0) to the local ion cyclotron frequency and fluctuation amplitudes $\delta B/B$ approximately 0.1 to 0.2 relative to the upstream field strength. The fluctuation amplitude in the transverse field components is typically a factor two larger than in the field magnitude. The observed wave properties are generally consistent with the simulation predictions that electromagnetic ion/ion cyclotron modes are excited by the beam-interaction between the upstream cold ions and the shock-heated, escaping downstream ions [Winske and Omid, 1990; Omid and Winske, 1992]. The observed wave amplitudes, however, are somewhat smaller than in the simulations.

The magnetic ramps in simulation slow shocks are typically of order $50 c/\omega_{pi}$, which corresponds to roughly $3 R_E$ in the distant tail. A single satellite, of course, cannot resolve space-time ambiguities, so we cannot determine the observed shock thickness. However, we can make the following estimate of the thickness based on the observed magnetic wave amplitudes. If we view the shock interaction in the deHoffman-Teller frame, the upstream ions flow along the magnetic field with velocity $v_{\parallel} = C_A$, the upstream Alfvén speed, assuming oblique switch-off shock conditions. Since the electric field vanishes in the deHoffman-Teller frame, the upstream ions have all the kinetic energy needed to produce the downstream temperature $T_2 = (\gamma - 1) m_i C_A^2 / 2 \gamma$ where γ is the adiabatic index. As the upstream ions enter the shock ramp and excite the ion cyclotron waves, they will be scattered essentially in pitch-angle to form the downstream heated distributions. For an approximate pitch-angle diffusion coefficient $D_{\alpha\alpha} = \Omega_i (\delta B/B)^2$ [Kennel and Petschek, 1966], we can write a phenomenological heating equation for the ions.

$$v_{||}(\partial T/\partial s) = D_{\alpha\alpha} [(\gamma-1)m_i C_A]^2 / 2\gamma - T]$$

where s is the distance along a field-line. Very roughly an upstream ion must travel a parallel distance $\Delta s \approx C_A / D_{\alpha\alpha} \approx c/\omega_{pi} (B/\delta B)^2 \approx 25 - 100 c/\omega_{pi}$. For switch-off shocks the shock thickness, λ , is roughly $\lambda \approx (B_2/B_1)\Delta s \approx 1/4 \Delta s \approx 8 - 25 c/\omega_{pi} \approx 0.5 - 1.5 R_E$ for the two February shocks. Given the very approximate nature of this estimate, the thicknesses of the tail slow shocks are probably somewhat smaller, but still comparable to the ramp thicknesses in the slow shock simulations.

The plasma waves consist of distinct mid-frequency and high frequency emissions. Within the shock ramp, the high frequency mode occurs between the maximum Doppler shift frequency and the local electron plasma frequency, has a quite low amplitude, and is strongly polarized with the electric field parallel to the magnetic field. At the top of the shock ramp, the broadband high frequency mode disappears, and is replaced by higher amplitude, impulsive narrowband electron plasma oscillations. The mid-frequency waves have a clear, fairly narrowband, spectral peak, which persists from upstream of the ramp through the shock transition. For one slow shock the peak frequency at the upstream edge was close to the electron cyclotron frequency but above the ion plasma frequency; for the other shock the peak frequency was unchanged even though the field strength was two times higher. The frequency of the spectral peak decreases through the ramp, and becomes comparable to both the down stream electron cyclotron and ion plasma frequencies. Thus the peak frequency does not appear to have any obvious relation to either the magnetic field strength (f_c) or the plasma density (f_{pi}). In addition, the peak frequency is anti-correlated with the maximum Doppler shift frequency, which increases from upstream to downstream. The mid-frequency emissions are highly impulsive, which renders difficult a clear determination of their electric field polarization. The only firm conclusion that we can draw is that the waves are not strongly polarized perpendicular to the field direction. The polarization distribution could be consistent with parallel polarization, but could also be compatible with a broad angular spread about the field direction.

The high frequency emission has not previously been identified as a distinct spectral component in either the broadband electrostatic noise in the near Earth plasma sheet [Gurnett *et al.*, 1976] or the plasma sheet and slow shock waves in the distant tail [Scarfi *et al.*, 1984; Coroniti *et al.*, 1990]. However, these emissions have essentially identical spectral anti polarization properties to a weak high frequency wave which occurs downstream of the low Mach number flank bow shocks [Coroniti *et al.*, 1993]. Although unaware of the high frequency emission being a distinct mode, Onsager *et al.* [1989] have suggested that waves between the ion and electron plasma frequencies

could be excited by very cold electron beams with speeds near or below the electron thermal speed. Alternatively *Coroniti et al.* [1993] proposed that discontinuities in the electron distribution function integrated over perpendicular velocities could support a non-standard, but beam-like wave mode which can be unstable if the distribution function increases across the discontinuity.

The strong similarity between the fast and slow shock high frequency emissions certainly suggests that their excitation mechanisms are similar. Furthermore, the slow shock wave observations lend support to these emissions being of electron origin. The emissions persist and follow the local magnetic field direction through the downstream region. Since the ion Larmor radius in the downstream field is large (of order 10^8 cm), the ion distribution should be isotropic and not sensitive to the local field direction. Thus, the ions are unlikely to contain the free energy which produces parallel polarized waves, whereas the electrons will remain magnetized, and a potential free energy source,

As for fast shocks, the electrostatic potential increases across slow shocks [*Schwartz et al.*, 1987]. Thus in slow shocks the upstream electrons are accelerated along the field by both the potential electric field and magnetic gradient force, which in the downstream distribution creates a velocity space separatrix between the trapped downstream electrons and the accelerated upstream electrons. *Feldman et al.* [1985] showed cuts of the downstream electron distribution function along zero perpendicular velocity which contained evidence for the separatrix, and perhaps a void at low parallel speeds. Since the distribution function is unlikely to always match smoothly at the separatrix, the non-standard, beam-like modes suggested by *Coroniti et al.* [1993] could exist in the downstream region of slow shocks and account for the observed high frequency emissions.

The origin of the micro-frequency emissions remains unclear. Since these modes are observed both in the upstream and ramp regions of the slow shock, the hole mode explanation of *Coroniti and Ashour-Abdalla* [1989] is probably not correct; in their model the hole at low electron energies occurred only upstream of the potential jump. The downstream electron distribution reported by *Feldman et al.* [1985] apparently has a hole at low energies; however, the distribution should be symmetric in parallel velocity so that no non-standard hole-type mode would occur. The mid-frequency waves fall in the frequency range of the broadband electrostatic noise found in the near Earth plasma sheet [*Gurnett et al.*, 1976], and thus could be generated by free energy in the ion distribution, but whether or not parallel cold ion beams [*Grabbe and Eastman*, 1984], perpendicular cold ion rings [*Huba et al.*, 1992], or hot ion beams [*Schrifer and Ashour-Abdalla*, 1987] exist in slow shocks cannot be determined with the ISEE 3 plasma instrument complement. However, the essential difficulty with all these instabilities is that, in order to obtain a solution to the dispersion

relation, the thermal speed of all ion components must be much less than the ion acoustic speed based on the electron temperature. Since T_e is almost always comparable to or less than T_i in the magnetosphere and magnetotail, the cold ion temperature constraint is very difficult to satisfy.

Recently *Onsager et al.* [1993] presented ISEE 1 and 2 observations of the plasma distributions and wave emissions in the near Earth plasma sheet boundary layer. They found, as did *Parks et al.* [1984], that the boundary layer has an outer region in which the electron distribution has enhanced fluxes and velocity space fine structure at energies above the thermal energy but the ion fluxes remained below the plasma instrument threshold, as in the lobes, and exhibited no evidence for field-aligned ion beams. The electron boundary layer contained intense wave emissions with a falling power spectrum from below the ion plasma frequency up to the electron plasma frequency; a deep spectral minimum occurred at the electron cyclotron frequency and a strong peak was positioned near the electron plasma frequency. When the spacecraft entered the ion boundary layer, the wave spectrum became a relatively featureless falling power law from low to high frequencies. *Onsager et al.* [1993] argue that boundary layer electrons alone can generate a broadband plasma wave spectrum at mid-frequencies without the necessity of involving ion beams; ion beams may only contribute to the low frequency portion of the spectrums.

The details of the electron region spectrum shown by *Ostinger et al.* [1993] differ from both the upstream and shock layer spectra for the February slow shocks; instead of the slow shock's clear mid-frequency spectral peak, the electron boundary layer emissions have only flattening of the spectrum. Nevertheless, *Onsager et al.*'s inference that broadband emissions can be generated by electrons alone may be relevant to the slow shock waves. We argued above that the high frequency waves are probably excited by electrons, perhaps by discontinuities in the downstream distribution function induced by the slow shock potential. Since the mid-frequency spectral peak is anti-correlated with the maximum Doppler shift frequency, these emissions either have long wavelengths ($k\lambda_D < 1/10 - 1/20$) to avoid Doppler shifting, or are not coupled to the flowing ion distribution, i.e., their dielectric function depends only on the electron distribution which implies a high phase speed. The phase speed can be expressed as

$$\omega/ka_e = (f/f_{pe})(2^{1/2}k\lambda_D)^{-1}$$

If we take $k\lambda_D = 0.1$ to avoid Doppler shifting by the high downstream flow, the mid-frequency spectral peak would have phase speeds in the range $\omega/ka_e \approx 0.1-0.2$, which is only 1.5 to 3.0 times greater than the downstream ion thermal speed, '1'bus, unless $k\lambda_D \ll 0.1$, the mid-

frequency modes would appear to have phase velocities which couple to the ions, and render the absence of Doppler shifting even more mysterious.

Acknowledgments. The work at TRW was supported by NASA Contracts NAS5-3 1827 (with NASA Headquarters) and NASW-4749 (with GSFC). The work at (California Institute of Technology, Jet Propulsion laboratory was supported by contract with NASA.

References

Anderson, R.R., C.C. Harvey, M. M. Hoppe, B. 'I'. Tsurutani, T.E. Eastman, and J. Etcheto, Plasma waves near the magnetopause, *J.Geophys.Res.*, 67, 208-, 1982.

Coroniti, F. V., F.L. Scarf, C. F. Kennel, B. 'I'. Tsurutani, and E. J. Smith, A search for lower hybrid drift turbulence. in slow shocks, *J.Geophys.Res.*, 93, 2.553, 1988.

Coroniti, F. V., and M. Ashour-Abdalla, Electron velocity space hole modes and narrowband electrostatic noise in the distant tail, *Geophys.Res.Lett.*, 16, 747, 1989.

Coroniti, F. V., E. W. Greenstadt, B. T. Tsurutani, E. J. Smith, R. D. Zwickl, and J. 'I'. Gosling, Plasma waves in the distant geomagnetic tail: ISEE 3, *J.Geophys.Res.*, 95, 20,977, 1990.

Coroniti, F. V., E. W. Greenstadt, S. I. Moses, E. J. Smith, and B. T. Tsurutani, Plasma waves downstream of weak collisionless shocks, *J.Geophys.Res.*, *in press*, 1993.

Feldman, W. C., S. J. Schwartz, S. J. Bame, D.N. Baker, J. Birn, J. T. Gosling, E. W. Hones, Jr., D. J. McComas, J. A. Slavin, E. J. Smith, and R. D. Zwickl, Evidence for slow-mode shocks in the deep geomagnetic tail, *Geophys.Res.Lett.*, 11, 599, 1984.

Feldman, W. C., D. N. Baker, S. J. Bame, J. Birn, J. T. Gosling, E. W. Hones, Jr., and S. J. Schwartz, Slow-mode shocks: A semipermanent feature of the distant geomagnetic tail, *J. Geophys.Res.*, 90, 233, 1985.

Gallagher, D. I., Short-wavelength electrostatic waves in the Earth's magnetosheath, *J.Geophys. Res.*, 90, 1435, 1985.

Grabbe, C.L., and "P. E. Eastman, Generation of broadband electrostatic waves in the magnetotail, *J. Geophys. Res.*, 89, 3865, 1984.

Gurnett, D. A., Plasma waves and instabilities, in *Collisionless Shocks in the Heliosphere Review of Current Research, Geophys. Mono. Ser., vol. 25*, ed. by B. T. Tsurutani and R. G. Stone, 207-224, AGU, Washington DC, 1985.

Gurnett, D. A., I. A. Frank, and R. P. Lepping, Plasma waves in the distant magnetotail, *J. Geophys. Res.*, 81, 6059, 1976.

Huba, J. D., J. Chen, and R. R. Anderson, Electrostatic turbulence in the Earth's central plasma sheet produced by multiple ring ion distributions, *J. Geophys. Res.*, 97, 1533, 1992.

Kennel, C. F., and H. E. Petschek, Limit on stably trapped particle fluxes, *J. Geophys. Res.*, 71, 1, 1966.

Omidi, N. and D. Winske, Kinetic structure of slow shocks: Effects of the electromagnetic ion/ion cyclotron instability, *J. Geophys. Res.*, 97, 14,801, 1992.

Onsager, P. G., R. H. Holzworth, H. C. Koons, O. H. Bauer, D. A. Gurnett, R. R. Anderson, H. Luhr, and C. W. Carlson, High frequency electrostatic waves near Earth's bow shock, *J. Geophys. Res.*, 94, 13,397, 1989.

Onsager, P. G., M. F. Thomsen, R. C. Elphic, J. "P. Gosling, R. R. Anderson, and G. Kettmann, Electron generation of electrostatic waves in the plasma sheet boundary layer, *J. Geophys. Res.*, 98, 15,509, 1993.

Parks, G. K., M. McCarthy, R. J. Fitzenreither, J. Etcheto, K. A. Anderson, R. R. Anderson, T. E. Eastman, I. A. Frank, D. A. Gurnett, C. Huang, R. P. Lin, A. "P, Y. Lui, K. W. Ogilvie, A. Pederson, H. Reme, and D. J. Williams, Particle anti field characteristics of the high-latitude plasma sheet boundary layer, *J. Geophys. Res.*, 89, 8885, 1984.

Richardson, I. G., S. W. H. Cowley, Plasmoid-associated energetic ion bursts in the deep geomagnetic tail: Properties of the boundary layer, *J. Geophys. Res.*, 90, 12,133, 1985.

Richardson, I. G., C.J. Owen, S. W. H. Cowley, A. B. Galvin, '1'. R. Sanderson, M. Scholer, J. A. Slavin, and R. D. Zwickl, ISFEE3 observations during the CDAW-8 intervals: Case studies of the distant geomagnetic tail covering a wide range of geomagnetic activity, *J. Geophys. Res.*, *94*, 15,189, 1989.

Rodriquez, P., Magnetosheath electrostatic turbulence, *J. Geophys. Res.*, *84*, 917, 1979.

Scarf, F. L., F. V. Coroniti, C.F. Kennel, E. J. Smith, J. A. Slavin, B. T. Tsurutani, S. J. Bame, and W. C. Feldman, Plasma wave spectra near slow mode shocks in the distant magnetotail, *Geophys. Res. Lett.*, *11*, 1050, 1984.

Schriver, D., and M. Ashour-Abdalla, Generation of high frequency broadband electrostatic noise; The role of cold electrons, *J. Geophys. Res.*, *92*, 5807, 1987.

Schwartz, S. J., M.F. Thomsen, W. C. Feldman, and F. J. Douglas, Electron dynamics and potential jump across slow mode shocks, *J. Geophys. Res.*, *92*, 3165, 1987.

Tsurutani, B. 'J', I. G. Richardson, R. M. Thorne, W. Butler, E. J. Smith, S. W. H. Cowley, S. P. Gary, S. I. Akasofu, and R. D. Zwickl, observations of the right-hand resonant ion beam instability in the distant plasma sheet boundary layer, *J. Geophys. Res.*, *90*, 12,159, 1985.

Winske, D., and N. Omidi, Electromagnetic ion/ion cyclotron instability at slow shocks, *Geophys. Res. Lett.*, *17*, 2297, 1990.

Winske, D., and N. Omidi, Electromagnetic ion/ion instability: Theory and simulations, *J. Geophys. Res.*, *97*, 14,779, 1992.

Figure Captions

Figure 1. Selected electric field spectral amplitudes (Volts/m- $\text{Hz}^{1/2}$) from 17.81 Hz to 100 kHz for the February 2, 1983 slow shock. The lower (upper) curves in each spectrum is the 30 second average (peak in 30 second interval) spectral amplitude in each frequency channel. The mid-frequency and high frequency emissions have clearly separated peaks in the 1920:50 UT spectrum.

Figure 2. Selected electric field spectral amplitudes for the February 11, 1983 slow shock.

Figures 3 a,b,c. High time resolution measurements for the February 2, 1983 slow shock. The top four panels display the vector components and magnitude of the magnetic field at 6 vectors/second resolution. Note the change in scale from Figure 3a to 3b and c. The bottom panels display the wave electric field measurements for the 56 Hz to 10 kHz channels; the scale is logarithmic and the 10^{-7} V/m- $\text{Hz}^{1/2}$ and 10^{-4} V/m- $\text{Hz}^{1/2}$ levels are indicated.

Figures 4 a,b. High time resolution measurements for the February 11, 1983 slow shock in the same format as Figure 3. Note the change in scale on the magnetic field magnitude panel from Figure 4 a to b.

Figure 5. The electric field polarization of the high frequency (3.16 kHz) emission during the February 2, 1983 slow shock. The radial scale is proportional to the logarithm (base 10) of the electric field spectral amplitude with a range of five decades. The sun is toward the left and dusk is toward the bottom of each diagram. Each polarization diagram contains two minutes of 240 electric field measurements. The ISHEE single-axis antenna is in the ecliptic plane and rotates about the ecliptic pole once every 3 seconds. The line labeled B is the ecliptic projection of the magnetic field; the magnetic field vector was essentially in the ecliptic plane throughout this interval.

Figure 6. The electric field polarization of the mid-frequency emissions for the February 2, 1983 slow shock. The format is the same as in Figure 5.

Figure 7. The electric field polarization of the mid-frequency (top) and high-frequency (bottom) emissions for the February 11, 1983 slow shock.

Figure 8. The electric field polarization of the mid-frequency (178 Hz and 316 Hz), high frequency (3.16 kHz), and electron plasma oscillations (5.62 kHz) in the I-amp (1920 UT) and upstream (1928 UT) regions of the February 2, 1983 slow shock. The inner circle represents the

average electric field spectral amplitude in the indicated frequency channel for the two minute interval. The outer curve assumes that the largest electric field amplitude measured during the two minute interval was produced by a parallel polarized signal, and represents the projection of that amplitude about the magnetic field direction in a dipole pattern. If the emissions are actually parallel polarized, no signals should occur outside this dipole projection curve.

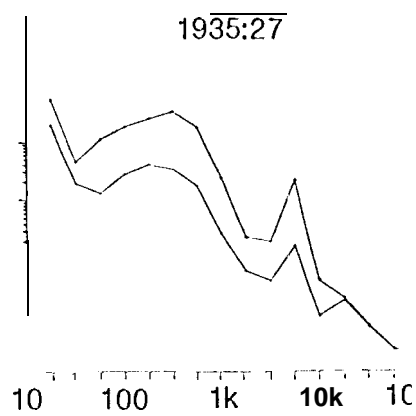
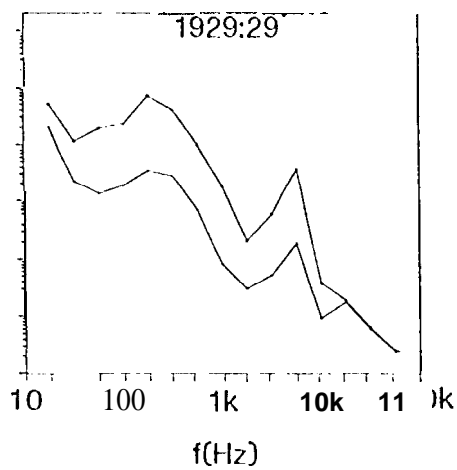
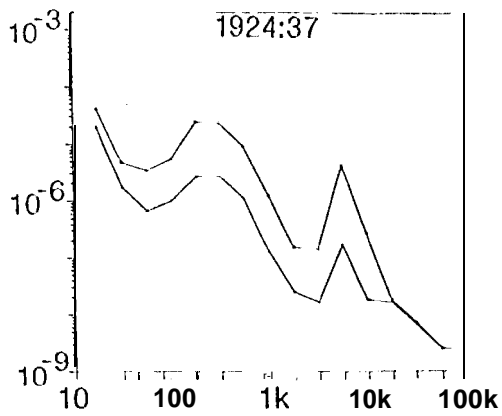
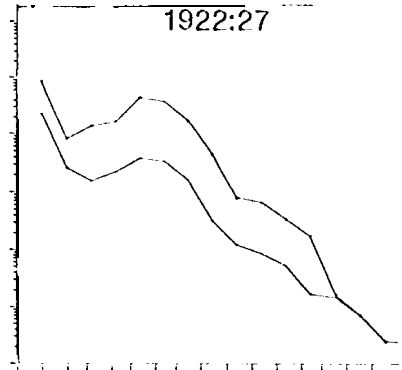
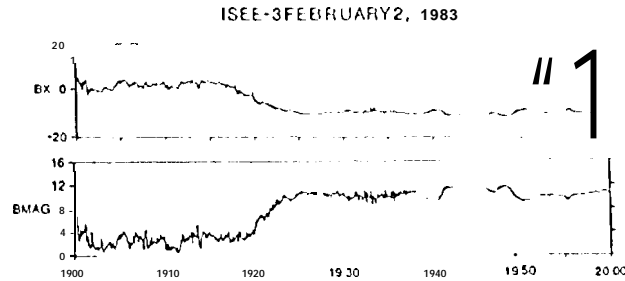
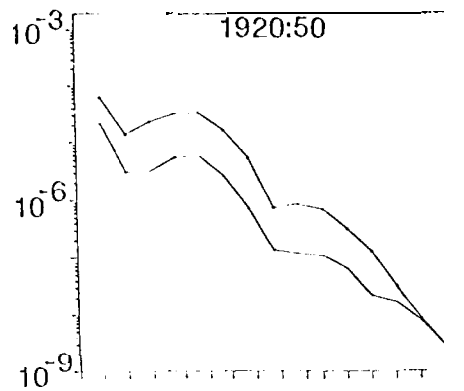
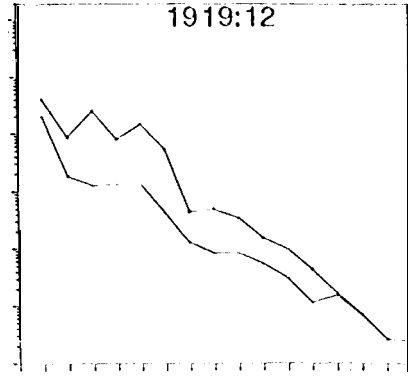
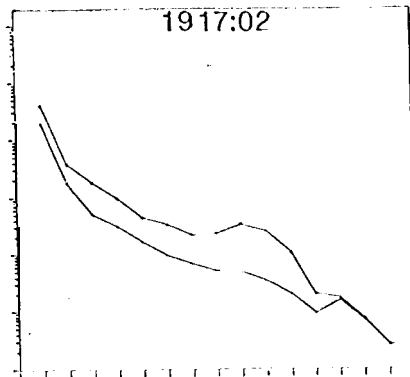
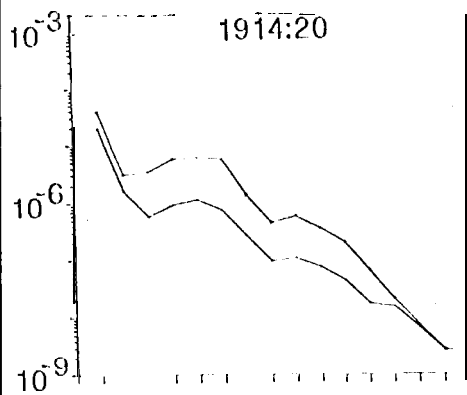


Fig. 1

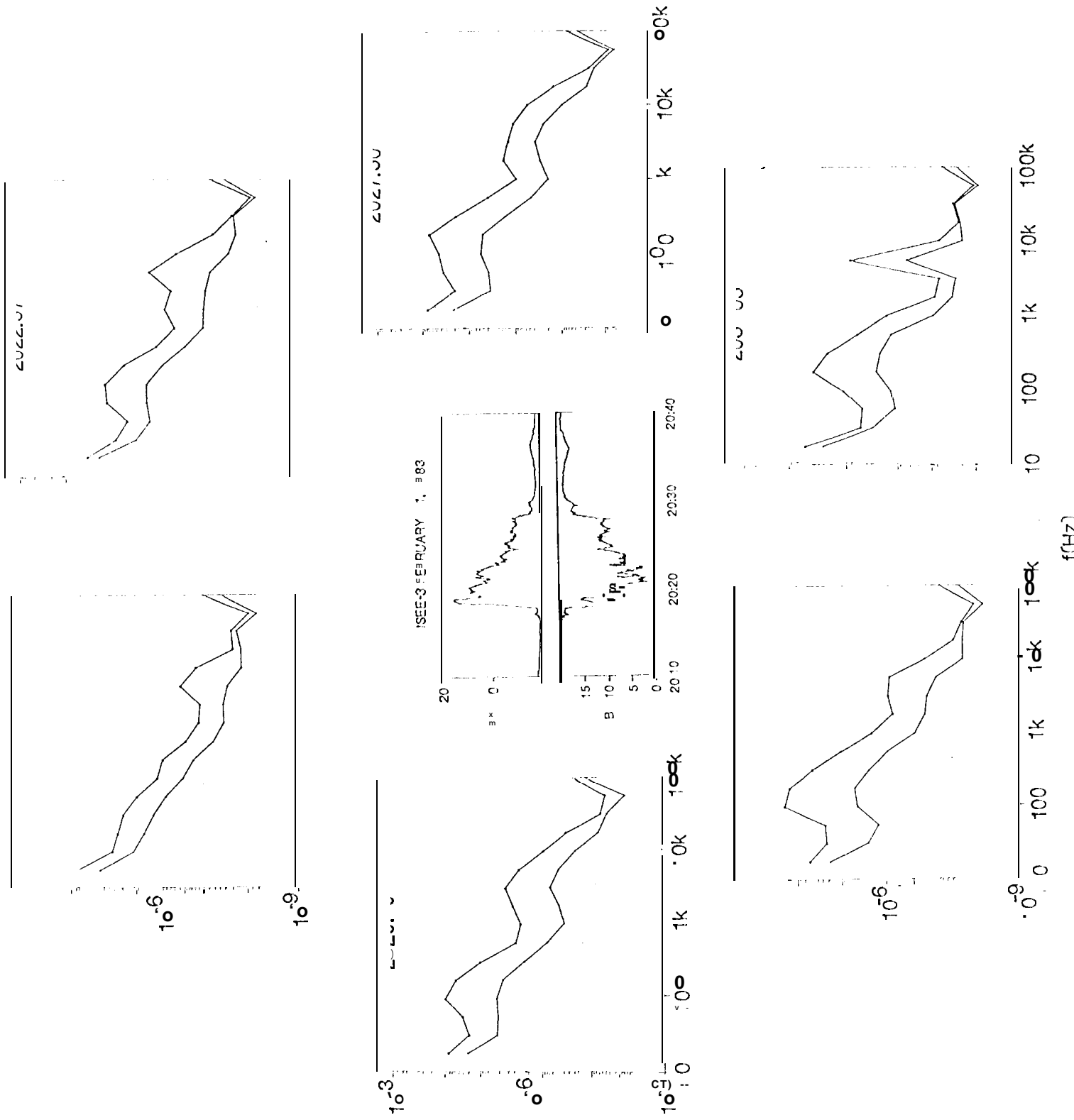


FIG 2

ISEE 3 February 2, 1983

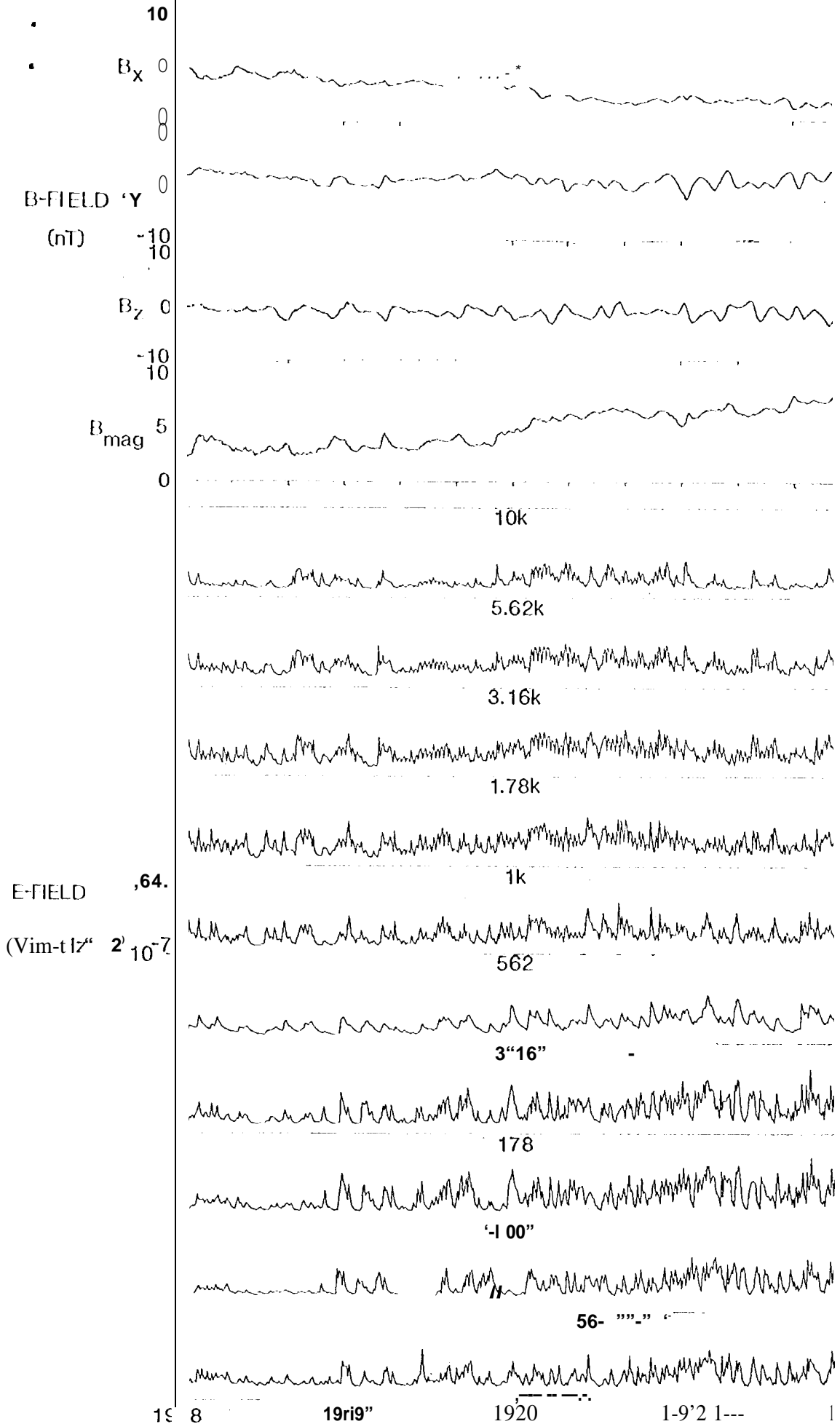


FIG 3a

ISEE-3 February 2, 1983

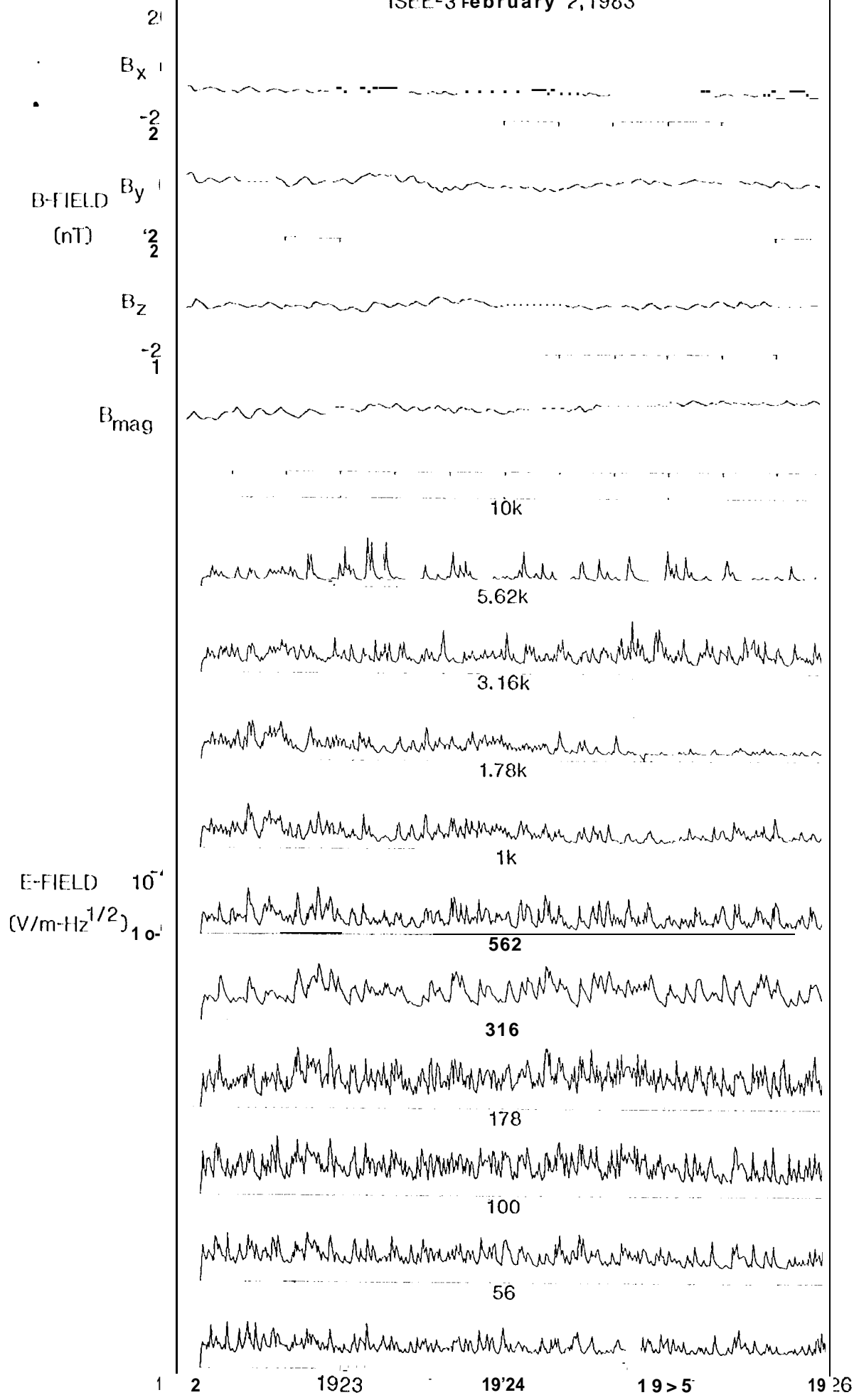


FIG 3b

ISEE 3 February 2, 1983

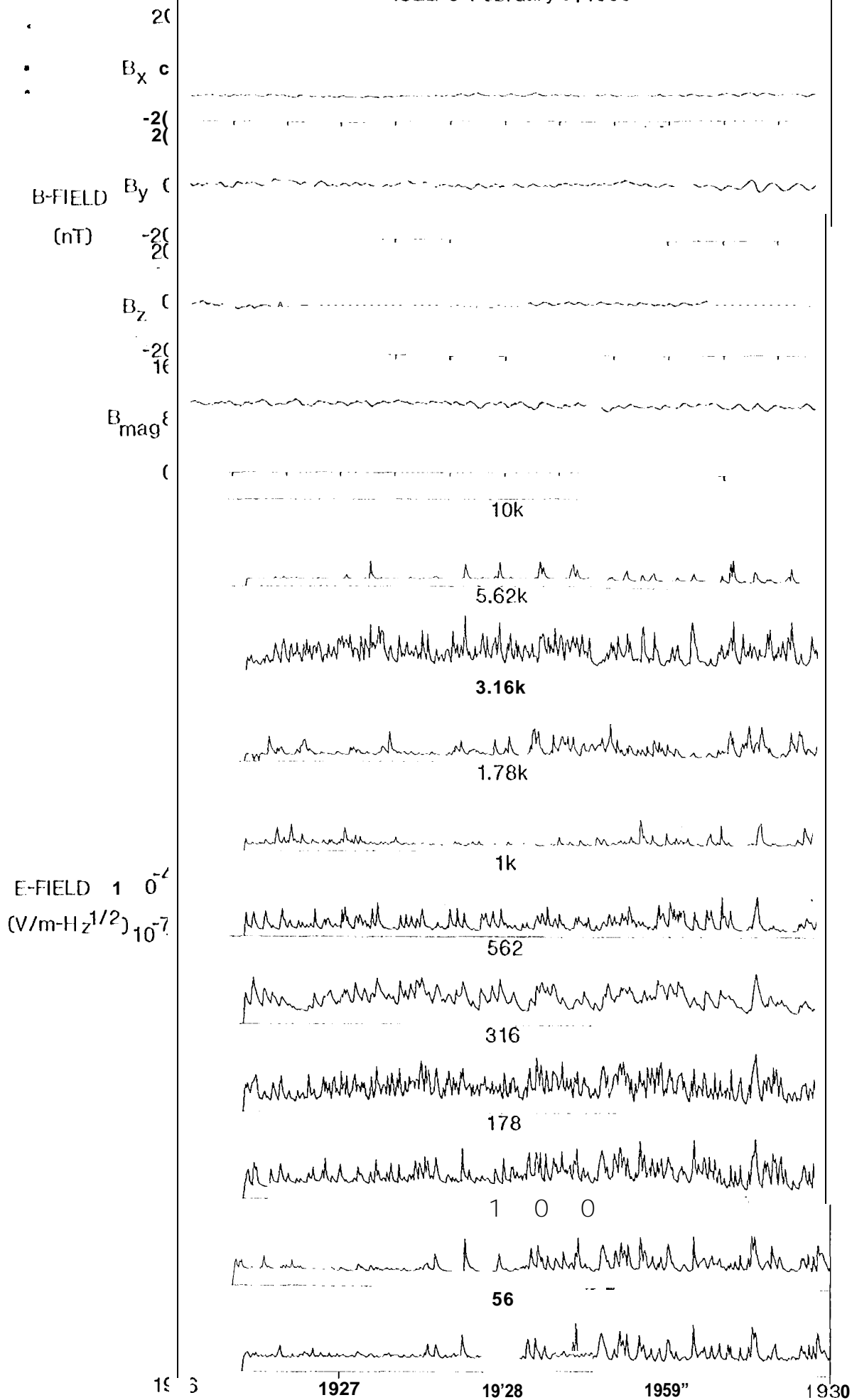


FIG 3c

ISEE 3 February 11, 1983

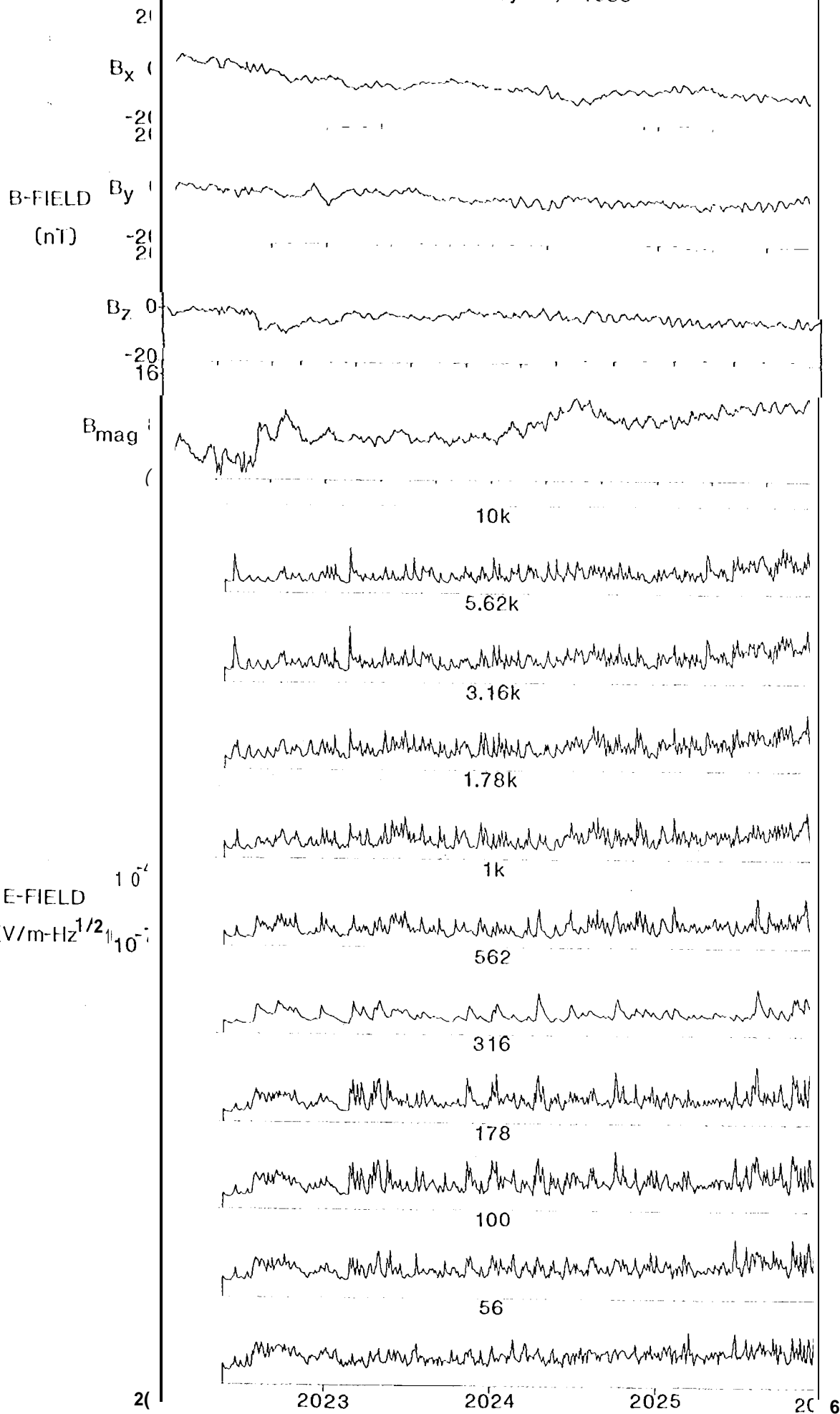


FIG 4a

ISEE 3 February 11, 1983

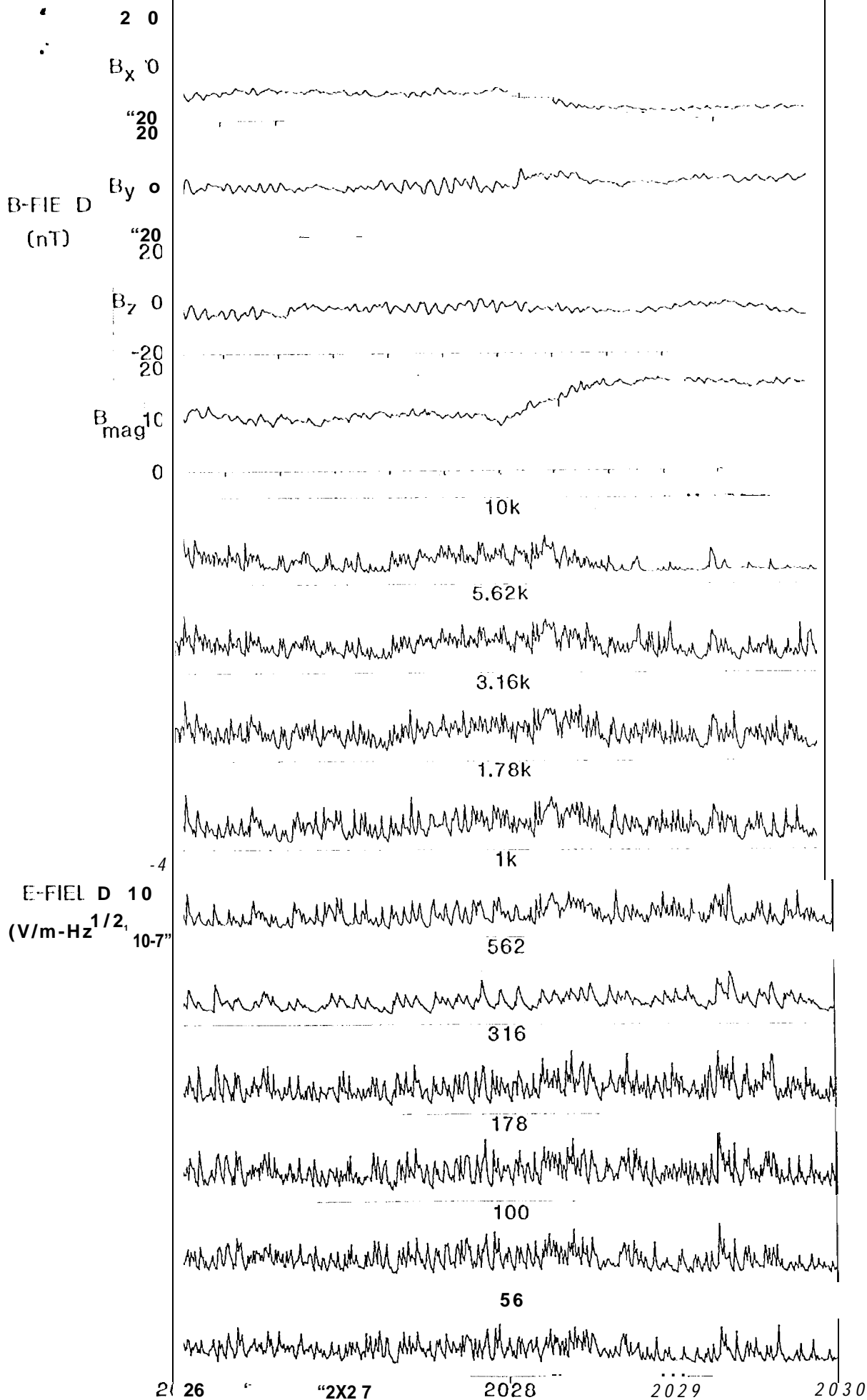
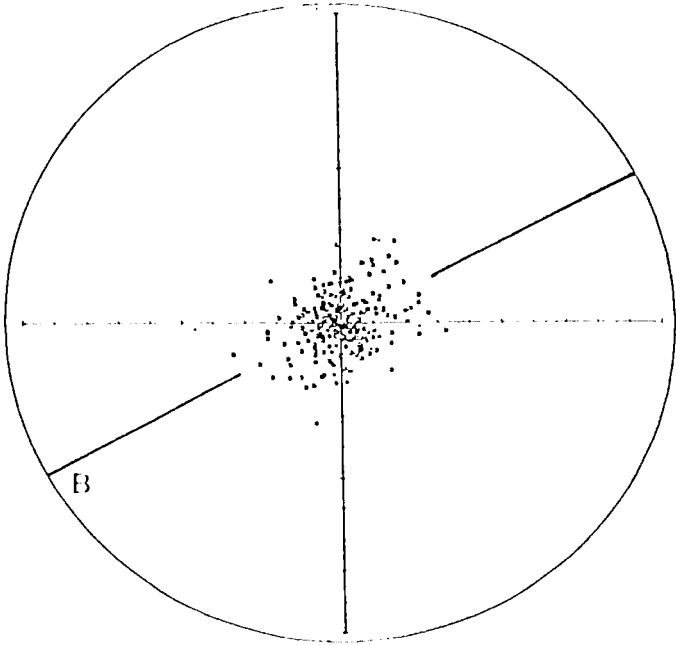
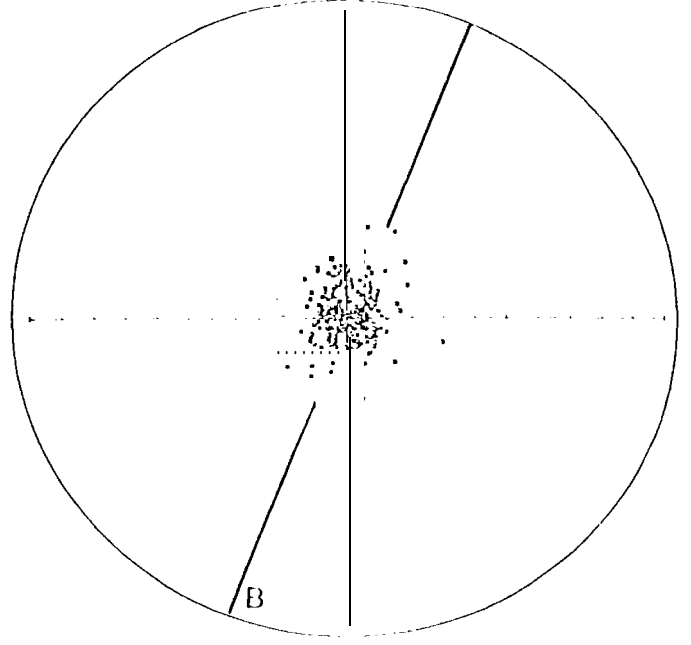


Fig 4b

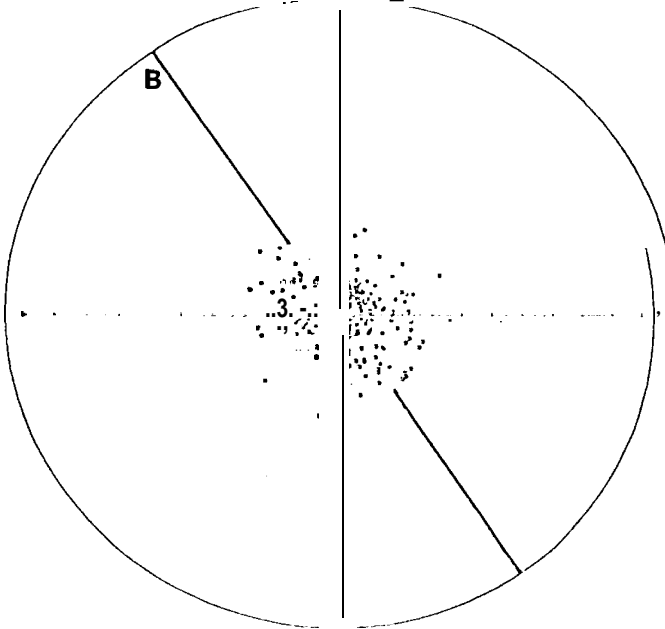
1914-1916



1916-1918

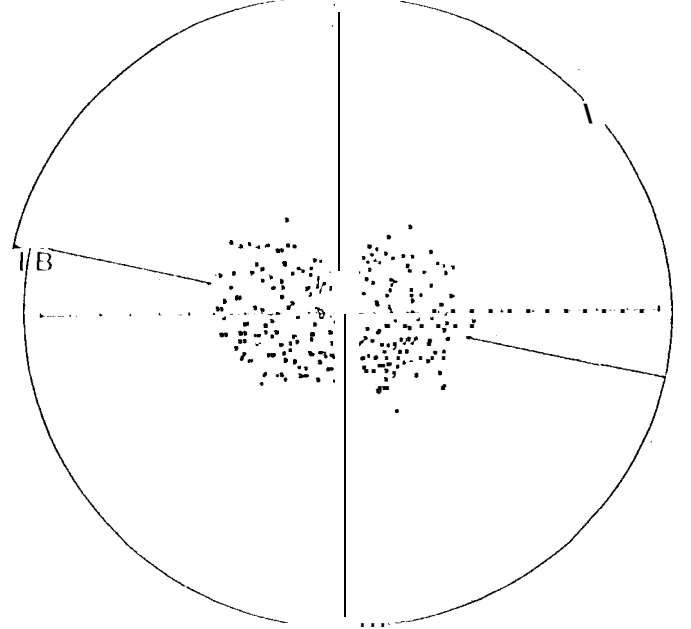


1918-1920

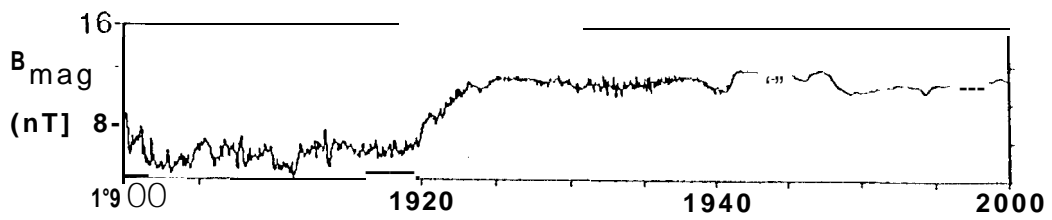


3.16 kHz

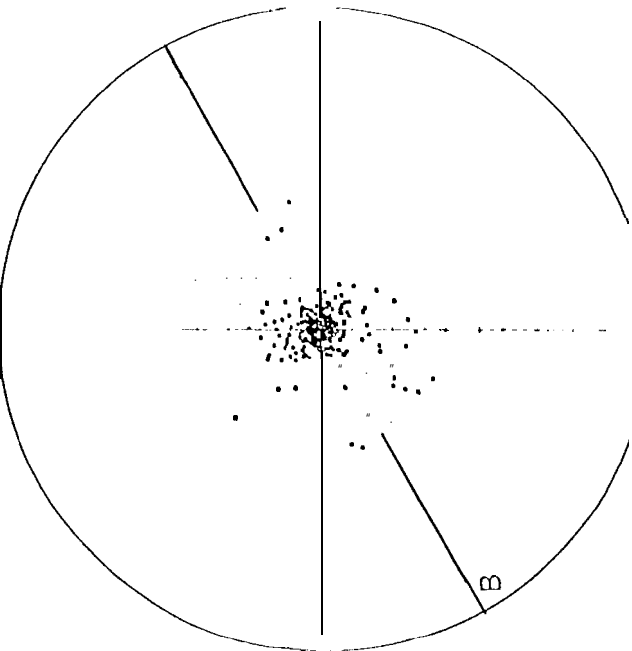
1920-1922



ISEE 3 February 2, 1983

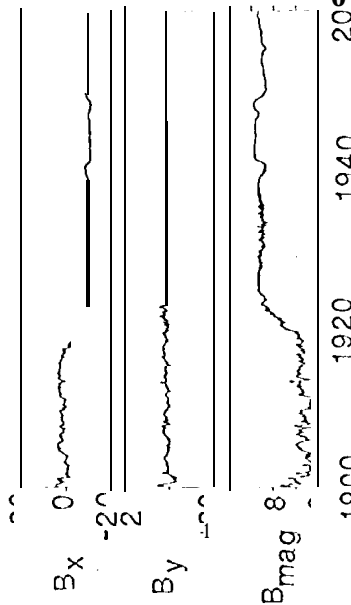


1914-1916



0.78 Hz

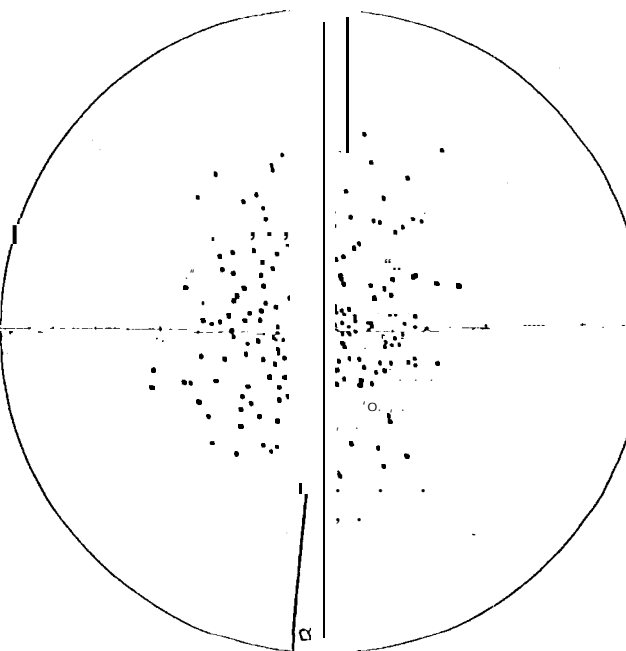
ISEE 3 February 2, 1983



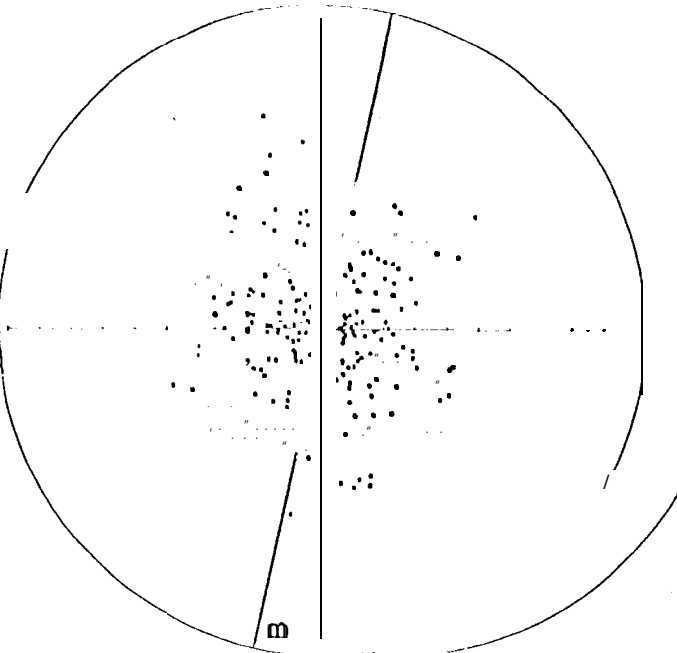
(nT)

3.6 Hz

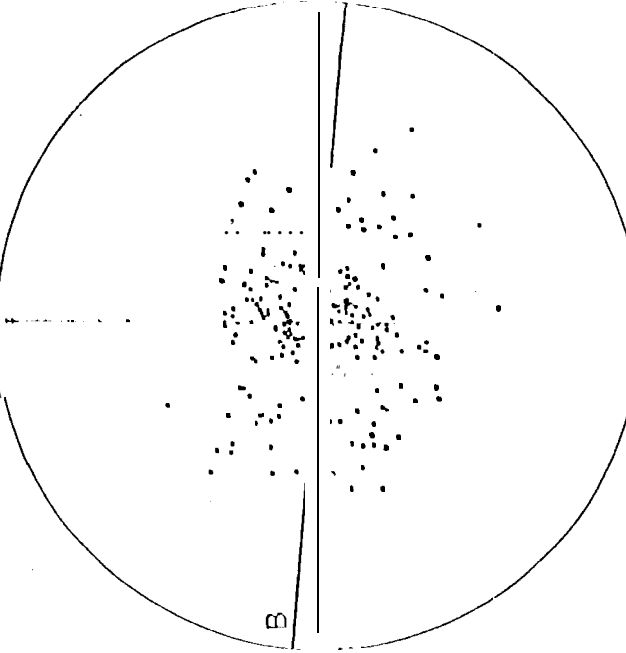
1924-1926



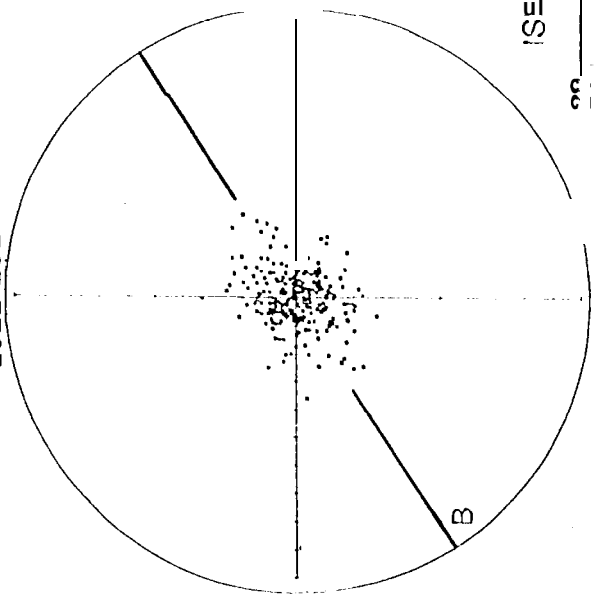
1920-1922



1928-1930

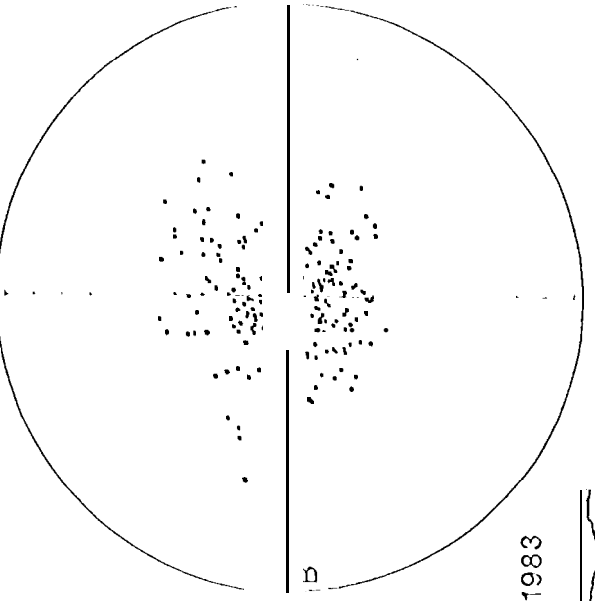


2022-2024

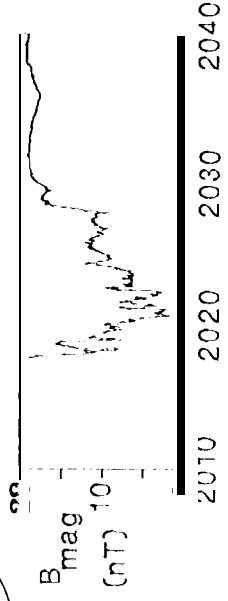


178 Hz

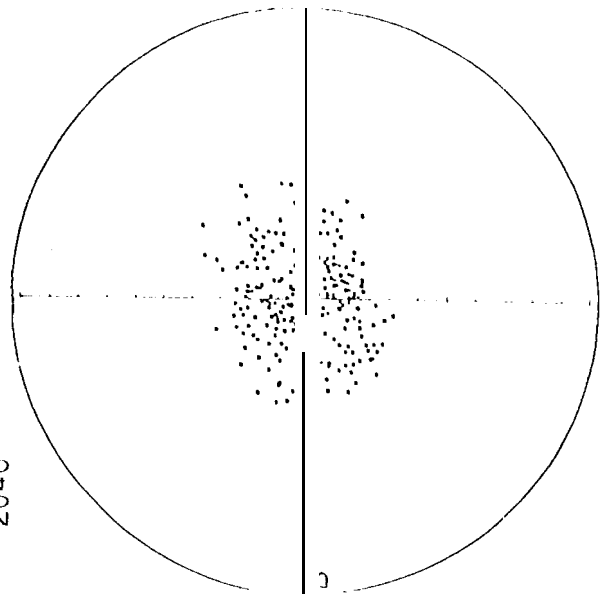
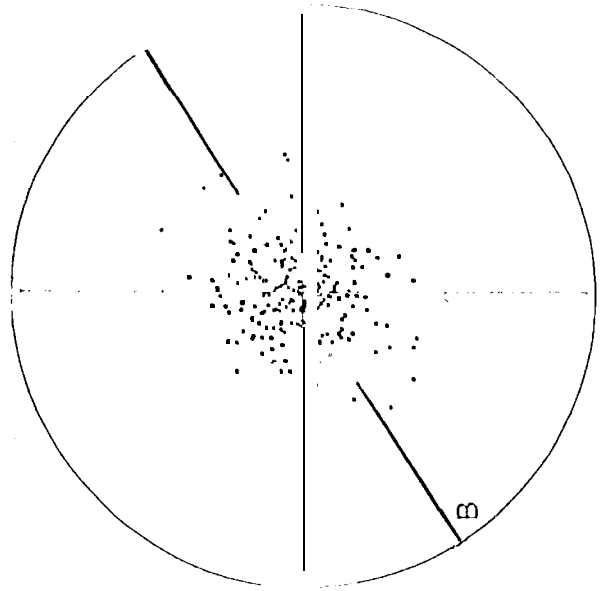
2026-2028

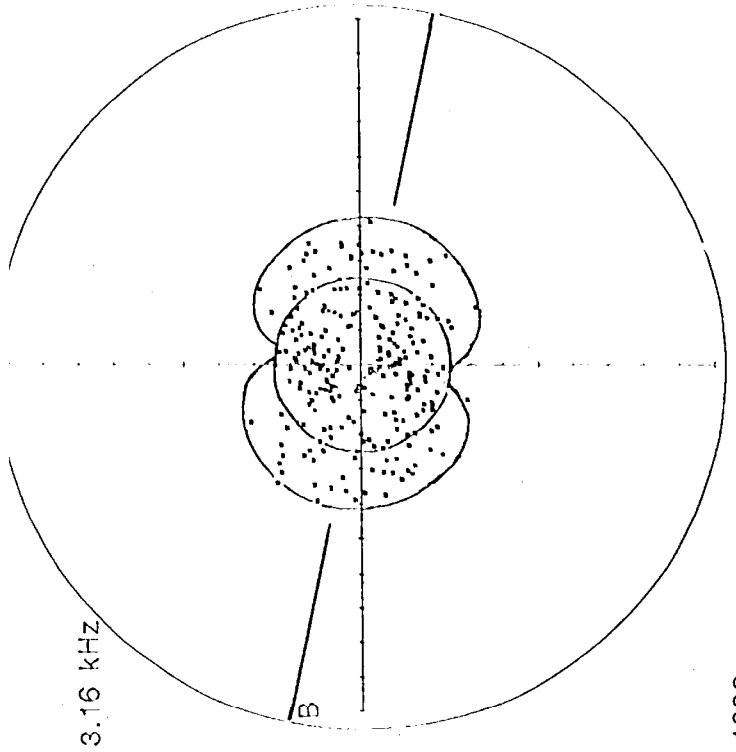
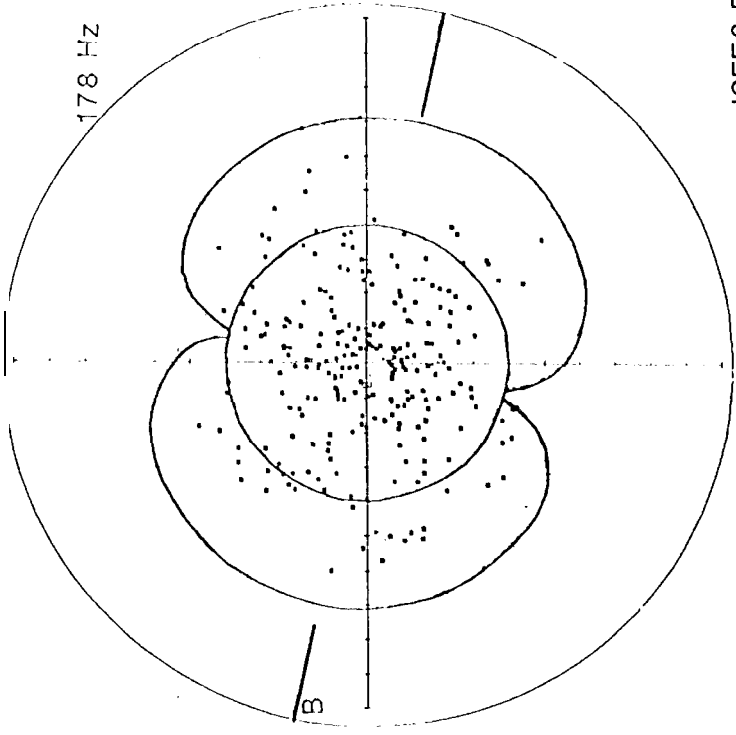


ISEE 3 February 11, 1983



3.16 kHz





ISEE3 February 2, 1983

